

## Article

# A Switched Capacitor-Based Single Switch Circuit with Load-Independent Output for Wireless Power Transfer

Bo Pan <sup>1</sup>, Houji Li <sup>1</sup>, Yong Wang <sup>1</sup> and Jianqiang Li <sup>2,\*</sup>

<sup>1</sup> Key Laboratory of Control of Power Transmission and Conversion, Ministry of Education, Shanghai Jiao Tong University, Shanghai 200240, China; panbost@sjtu.edu.cn (B.P.); lihoushen@sjtu.edu.cn (H.L.); wangyong75@sjtu.edu.cn (Y.W.)

<sup>2</sup> Shanghai Academy of Spaceflight Technology, Shanghai 201109, China

\* Correspondence: lijianqiang@805.sast.casc

**Abstract:** Double-sided Inductor–Capacitor–Capacitor (LCC) or hybrid compensation network is often used in the traditional methods to realize load-independent output in wireless power transfer; however, these methods require the changes of operating frequency or compensation network, and the adoption of more switches and components, resulting in the reduction in the reliability of the system. In this article, a single switch topology using a switched capacitor was proposed, which can realize load-independent output characteristics by only switching the branch once, characterized by the strength of fewer components, simple control, and high reliability. The analysis of this topology and the accurate parameter design method were given, and the sensitivity analysis was also carried out. Finally, a 180 W wireless charging prototype with 60 V/3 A was built using the proposed topology, which confirmed the accuracy of model analysis and the practical feasibility of the proposed strategies.

**Keywords:** load-independent output; single switch; higher-order harmonics; wireless power transfer



**Citation:** Pan, B.; Li, H.; Wang, Y.; Li, J. A Switched Capacitor-Based Single Switch Circuit with Load-Independent Output for Wireless Power Transfer. *Electronics* **2022**, *11*, 1400. <https://doi.org/10.3390/electronics11091400>

Academic Editor: Sheldon Williamson

Received: 16 March 2022

Accepted: 26 April 2022

Published: 27 April 2022

**Publisher's Note:** MDPI stays neutral with regard to jurisdictional claims in published maps and institutional affiliations.



**Copyright:** © 2022 by the authors. Licensee MDPI, Basel, Switzerland. This article is an open access article distributed under the terms and conditions of the Creative Commons Attribution (CC BY) license (<https://creativecommons.org/licenses/by/4.0/>).

## 1. Introduction

Wireless power transfer (WPT) is a method used for transferring power by coupling the magnetic fields of the transmitting and receiving coils. It is characterized by multiple inherent strengths, e.g., security, convenience, reliability, electrical isolation, low cost, no need for bulky wires and heavy connectors, and the ability to be applied in extreme environments and special applications. These merits make WPT increasingly widely recognized and studied. According to different principles, WPT can be classified into three forms, i.e., magnetic field coupling power transfer, electric field coupling power transfer, and microwave wireless power transfer. Nowadays, magnetic field coupling power transfer is popular in electrical vehicle (EV) wireless charging, aerospace and ocean exploration, household appliances, and so on [1,2].

Currently, in the medium to high power applications of WPT, full-bridge inverter topology is generally adopted [3]. The scheme of the full-bridge inverter circuit is mature; however, the inverter consists of four switches, which leads to the disadvantages of large volume and heavy weight, complex control, poor reliability, and difficulty to realize zero voltage switching (ZVS) [4,5]. Single switch circuit, e.g., Class E circuit, is widely adopted in the field of low-power WPT because of its merits of fewer components, simple control, and zero voltage switching, but the conventional Class E topology can be utilized only in low-power situations due to high voltage stress [6–8]. In [9], the author reveals a reconfigurable Class E topology-based wireless power transmitter of 6.78 MHz. This proposed topology in [9] enjoys the benefits of charging different types of multi-components while remaining very high efficiency; however, the transmission power of 39 W greatly limits the application of the Class E circuit.

In this paper, a hybrid topology of the Class E circuit, which can realize bidirectional excitation, is proposed. The proposed topology can transmit energy to the load no matter whether the switch is on or off, which improves the utilization of the power source. In addition, the power transmission level is increased from several hundreds of watts to thousands of watts, thus greatly improving the power transmission capacity of the circuit. Moreover, this novel topology achieves load-independent output characteristics by switching the branch only once. It is of significance to realize load-independent output to extend the life span of batteries in wireless battery-charging applications [10]. Nowadays, load-independent output in a WPT system is usually achieved by the addition of a double-sided Inductor–Capacitor–Capacitor (LCC) compensation network to a full-bridge inverter topology [11–13]. In [14], the authors recommend a double-sided LCC compensation network for the WPT system, as well as a tuning approach for it. The resonant frequency of the circuit in [14] is unaffected by both the coupling coefficient between coils and the load conditions. In low to mid-power applications, however, it necessitates more passive components, resulting in bigger system sizes, more resonant loops, and worse efficiency. Furthermore, as the switching frequency of the circuit must be altered when the system is switched between constant current (CC) and constant voltage (CV) modes, its stability has reduced. Authors presented two hybrid circuits for electric vehicle charge in [15], employing either SS (Series–Series) and PS (Parallel–Series) compensation or SP (Series–Parallel) and PP (Parallel–Parallel) compensation. Although this method is available to convert between CC and CV modes without modifying the operating frequency, the circuit topology is complicated since there are three switching switches. In addition, the new resonant loop modified the previous compensation circuit; therefore, it is important to find a simple topology structure to realize CC and CV output at a fixed switching frequency. In [16], a full-bridge circuit and a primary reconfiguration of the compensation network are used, and the CC and CV modes can be implemented by switching only once, but more passive devices are used, which is not suitable for applications with small transmitter reflection impedance.

This novel Class E topology presented in this paper has a Series/Capacitor–Inductor–Capacitor (S/CLC) structure, which reduces the number of passive components. In addition, to transition between CC and CV mode, only one switch is required, with no changes to the compensation network. Compared with full-bridge topology, this presented Class E topology has the strength of high stability, small volume, and light weight, simple structure, and control. In addition, it is simple to achieve ZVS and there are no issues with shoot-through [17,18]. Moreover, this output power is no longer limited to a few watts; instead, it can reach hundreds of watts, thereby expanding its range of application in medium power.

## 2. Analysis of a Novel Class-E Topology

### 2.1. Topology of Main Circuit

To solve the above problems, a novel Class E topology and S/CLC compensation network are presented, as shown in Figure 1. The transmitter circuit is a basic Class E topology; the receiver circuit adopts a CLC compensation network and a bridge rectifier topology, which requires no change of operating frequency and compensation network, and only needs to switch the branch once to achieve load-independent output. In addition, it enables ZVS to meet the need for mid-power and small power applications.

This proposed topology consists of an inverter unit, a magnetically coupled structure, and a high-frequency rectifier. Among them, the Class E unit is composed of  $L_1$ ,  $Q$ ,  $C_1$ , which transforms the input DC power into high-frequency AC power. The magnetically coupled structure is composed of  $L_p$ ,  $C_p$ ,  $L_s$ ,  $C_{s1}$ ,  $C_{s2}$ ,  $C_{s3}$ ,  $S$ , and  $L_2$ , which transmits power from the transmitting circuit to the receiving circuit through a magnetic field. In the case that the switch  $S$  is closed, the receiving side capacitors are  $C_{s1}$ ,  $C_{s2}$ ; the system works in CC mode; when the switch  $S$  is on, the receiving side capacitors are a combination of  $C_{s1}$  and  $C_{s3}$  in parallel, and the system works in CV mode. The switch  $S$  is not a high-frequency switch, so it only needs to be switched once in the process of charging the battery. The high-

frequency rectifier is a full-bridge rectifier, composed of four diodes, that can transform the high-frequency AC power to DC power and supply the load.

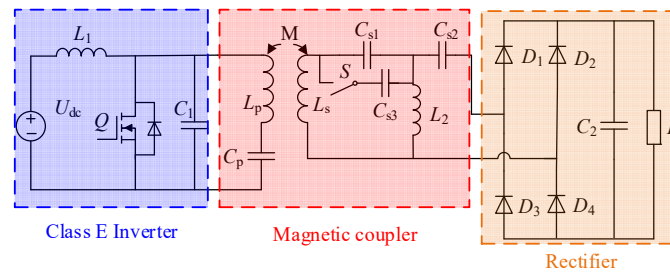


Figure 1. The presented novel Class E topology.

Figure 2 shows the working process waveform of the Class E inverter using Saber simulation. Here  $u_{gs}$ , refers to voltage through the gate source of the switch Q;  $u_{ds}$  stands for voltage across the drain source of the switch Q;  $i_{Lp}$  and  $i_{Ls}$  represent the current in the transmitting and receiving coil, respectively,  $u_{Cs1}$  and  $u_{Cs2}$  are the voltage waveform on capacitor  $C_1$  and  $C_2$ ;  $u_{L1}$  and  $i_{L1}$  denote the voltage and current waveforms on inductor  $L_1$ , respectively.

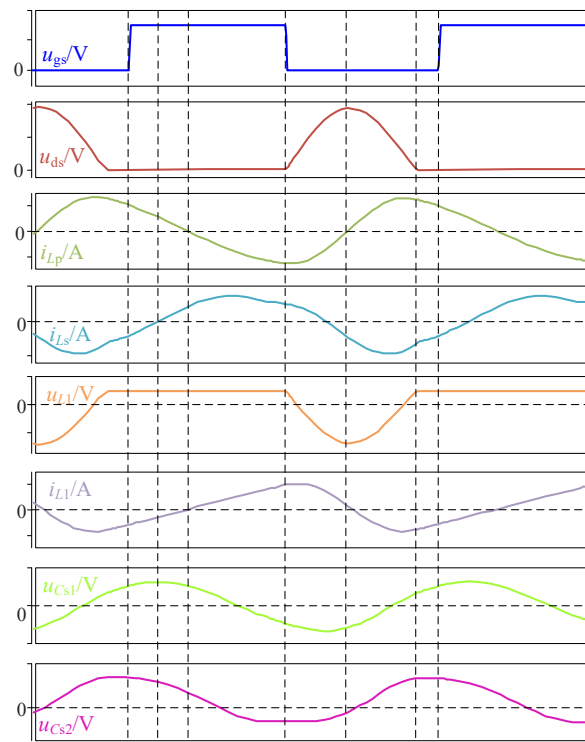


Figure 2. The working process waveform of inverter unit.

From Figure 2, it can be seen that when  $u_{ds}$  goes to zero, therefore, the switch S exhibits the zero-voltage switching characteristic.

### 2.2. Constant Current Output Mode

As shown in Figure 3, a T-type equivalent network is used to analyze the magnetically coupled structure of the Class E topology.

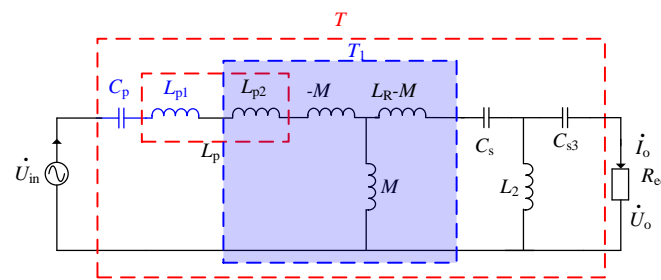


Figure 3. T-type equivalent network.

As can be seen from Figure 3, the primary inductor  $L_p$  is decomposed into  $L_{p1}$  and  $L_{p2}$ , respectively.  $C_p$  compensates for the partial inductance of the transmitting coil  $L_{p1}$ , so that the T1 network can achieve the voltage source to the voltage source (V–V) transformation [19].  $C_s$  refers to the secondary compensation capacitor and its value is subject to the state of the switch S. On the other hand,  $u_{in}$  is expressed as a sine wave input voltage, the load is approximated as a pure resistance  $R_{eq}$ , the output voltage before rectification is  $U_o$ , and the output current is  $I_o$ . Due to the fact that capacitor  $C_1$  is in parallel with the voltage  $u_{in}$ , it does not affect CC and CV of the compensation network. Capacitor  $C_1$  only affects the ZVS characteristics of the system.

It is assumed that the system realizes CC output only at the frequency  $f$ . Moreover, in cases where the transmitting coil compensation capacitor  $C_p$  and inductor  $L_{p1}$  are resonant at this frequency, the total impedance of  $C_p$  and  $L_{p1}$  becomes zero. According to Thévenin’s and Norton’s theorem, the T1 network shown in Figure 3 could be equivalent to an inductor, given in Figure 4a. In case the equivalent inductor  $L_s - M^2/L_{p2}$ ,  $C_{s1}$  and  $L_2$  resonate at  $f$ , the structure shown in Figure 4b can be obtained.

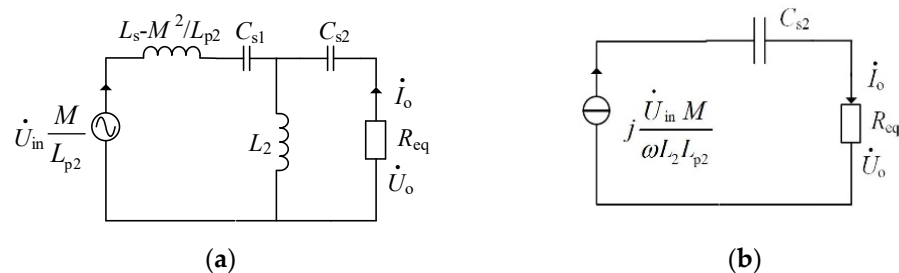


Figure 4. Equivalent circuit in CC mode. (a) Equivalent model. (b) Final equivalent model.

It is shown in Figure 4b that the magnetically coupled structure is equivalent to a constant current source in series with capacitor  $C_{s2}$  and equivalent resistance  $R_{eq}$ . In other words, the CC output mode is achieved. According to the previous analysis, the circuit needs to meet the following requirements to realize constant current output:

$$\begin{cases} \omega L_{p1} = \frac{1}{\omega C_p} \\ \omega \left( L_s - \frac{M^2}{L_{p2}} \right) - \frac{1}{\omega C_{s1}} = -\omega L_2 \end{cases} \quad (1)$$

where  $\omega = 2\pi f$ . Through the aforementioned analysis, at the switching frequency of  $f$ , the calculation of the compensation network output current can be expressed:

$$I_o = \frac{j\omega C_{s1} U_{in} M}{L_{p2} - \omega^2 C_{s1} (L_s L_{p2} - M^2)} \quad (2)$$

From (2), it can be seen that the compensation network output current of the CC mode is subject to the voltage  $U_{in}$ , inductor  $M$ ,  $L_s$ ,  $L_{p2}$ , and capacitor  $C_{s1}$ . Where  $L_{p2}$  can be separated from the inductor  $L_p$ ; therefore, this design approach significantly enhances the design freedom of the system.

### 2.3. Constant Voltage Output Mode

At the CV output mode, the secondary compensation capacitor  $C_s$  is the combination of  $C_{s1}$  and  $C_{s3}$  in parallel, i.e., the switch S is turned on. As seen in Figure 4a, If the inductor  $L_s - M^2/L_{p2}$ ,  $L_2$  and  $C_{s1}$  are combined in parallel to resonate with  $C_{s2}$  at switching frequency  $f$ , an equivalent circuit can be given as shown in Figure 5.

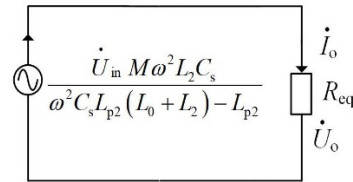


Figure 5. Equivalent model in CV mode.

Figure 5 shows that the magnetically coupled structure is equivalent to a constant voltage in series with equivalent resistance  $R_{eq}$ ; therefore, the voltage across  $R_{eq}$  is dependent on the value of resistance, which achieved constant current output. According to the previous analysis, the circuit needs to meet the following requirements to realize constant voltage output:

$$\begin{cases} C_s = C_{s1} + C_{s3} \\ (j\omega L_0 + \frac{1}{j\omega C_s}) // j\omega L_2 + \frac{1}{j\omega C_{s2}} = 0 \\ L_0 = L_s - M^2/L_{p2} \end{cases} \quad (3)$$

where  $\omega = 2\pi f$ . Through the aforementioned analysis, at the switching frequency of  $f$ , the calculation of the compensation network output voltage can be expressed:

$$\dot{U}_o = \frac{\dot{U}_{in} M \omega^2 L_2 C_s}{\omega^2 C_s L_{p2} (L_0 + L_2) - L_{p2}} \quad (4)$$

From (3), the expression of the compensation capacitor  $C_{s2}$  can be reformulated as:

$$C_{s2} = \frac{1 - \omega^2 C_s (L_0 + L_2)}{\omega^2 L_2 (1 - \omega^2 L_0 C_s)} \quad (5)$$

### 3. Parameter Analysis

The AC output current and voltage are rectified using a full-bridge diode rectifier; the current  $I_b$  and voltage  $U_b$  can be obtained as follows:

$$\begin{cases} I_b = \frac{2}{\pi} I_o \\ U_b = \frac{\pi}{4} U_o \end{cases} \quad (6)$$

To simplify the calculation, the variables  $\alpha$ ,  $\beta$ , and  $k$  are introduced, which can be expressed as:

$$\begin{cases} L_{p2} = \alpha L_p \\ k = \frac{M}{\sqrt{L_p L_s}} \\ C_{s1} = \beta C_s \end{cases} \quad (7)$$

Substituting (2), (4), and (7) into (6), expressing  $\omega$  with  $\alpha$ ,  $\beta$ , and  $k$  can be obtained as:

$$\omega = \frac{2U_b I_b L_p \alpha^2 (1 - \beta)}{U_{in}^2 k^2 C_s L_s \beta} \quad (8)$$

For the application of 48 V, 20 AH battery, the proposed Class E topology is designed with the parameters of 100 V input voltage and 60 V/3 A output voltage and current, and the parameters of the whole system may be calculated according to the above analysis.

Given a set of transmitting coil and receiving coil, for example,  $L_p = 20 \mu\text{H}$ ,  $L_s = 30 \mu\text{H}$ . From Figure 6, the switching frequency  $f$  versus the coupling coefficient  $k$  for different  $\alpha$  and  $\beta$  can be derived.

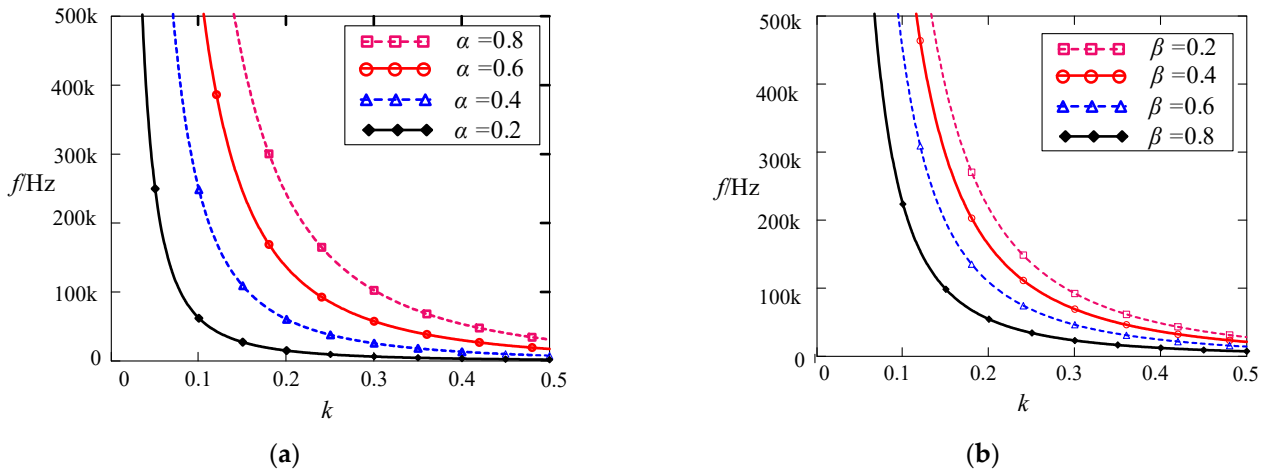


**Figure 6.** (a) switching frequency  $f$  versus the coupling coefficient  $k$  when  $\alpha$  changes; (b) switching frequency  $f$  versus the coupling coefficient  $k$  when  $\beta$  changes.

From Figure 6, it may be observed that for a certain switching frequency, the required value of  $\alpha$  becomes larger, and the value of  $\beta$  becomes smaller with the increase in the coupling coefficient; however, the maximum value of  $\alpha$  is 1; therefore, the system parameters are limited by  $f$  and  $k$ . The higher the  $f$ , the smaller the feasible range of  $k$ . At given  $f$  and  $k$ , the coefficients  $\alpha$  and  $\beta$  can be determined from Figure 6.

To show the relationship between parameters  $\alpha$ ,  $\beta$ , and frequency  $f$ , a three-dimensional image was created, as shown in Figure 7.

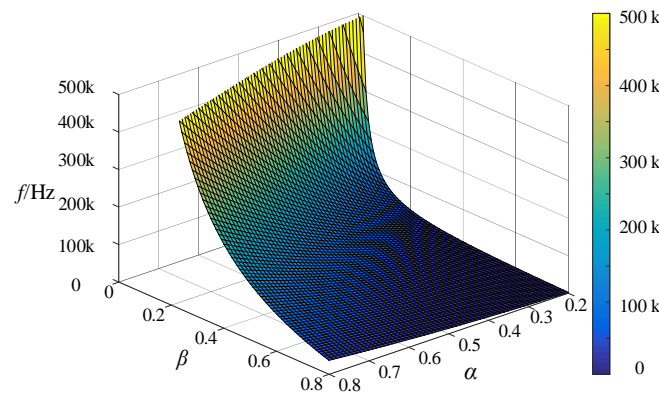


**Figure 7.** The relationship between parameters  $\alpha$ ,  $\beta$ , and frequency  $f$ .

All parameters of the topology can be calculated by analyzing the above figures and formulas; therefore, the parameters of the novel Class E topology and its compensation network are calculated as illustrated in Table 1.

Sensitivity analysis of the topology was performed in order to verify the sensitivity of the system at this parameter. The variation of CV-mode normalized output voltage and CC-mode normalized output current with  $C_s$ ,  $\alpha$  and  $L_2$  normalization parameter is shown in Figure 8. It is obvious that the change of  $C_s$  is sensitive to the output current. At the same time, the value of  $L_2$  is not sensitive to the variation of constant voltage output.

**Table 1.** Class E topology parameter.

Parameter	Description	Value
$f$	frequency	100 kHz
$U_{dc}$	Input DC voltage	100 V
$U_b$	Output voltage	60 V
$I_b$	Output current	3 A
$L_p$	Transmitting coil inductance	20 $\mu$ H
$L_s$	Receiving coil inductance	30 $\mu$ H
$M$	Mutual inductance	6.12 $\mu$ H
$\alpha$	Scale factor	0.61
$\beta$	Scale factor	0.5
$C_p$	Primary compensation capacitor	324.7 nF
$C_s$	Compensation capacitor in CV mode	98 nF
$C_{s1}$	Compensation capacitor in CC mode	49 nF
$C_{s2}$	Secondary compensation capacitor	768 n
$L_1$	Primary side inductance	16 $\mu$ H
$L_2$	Secondary side inductance	24.5 $\mu$ H

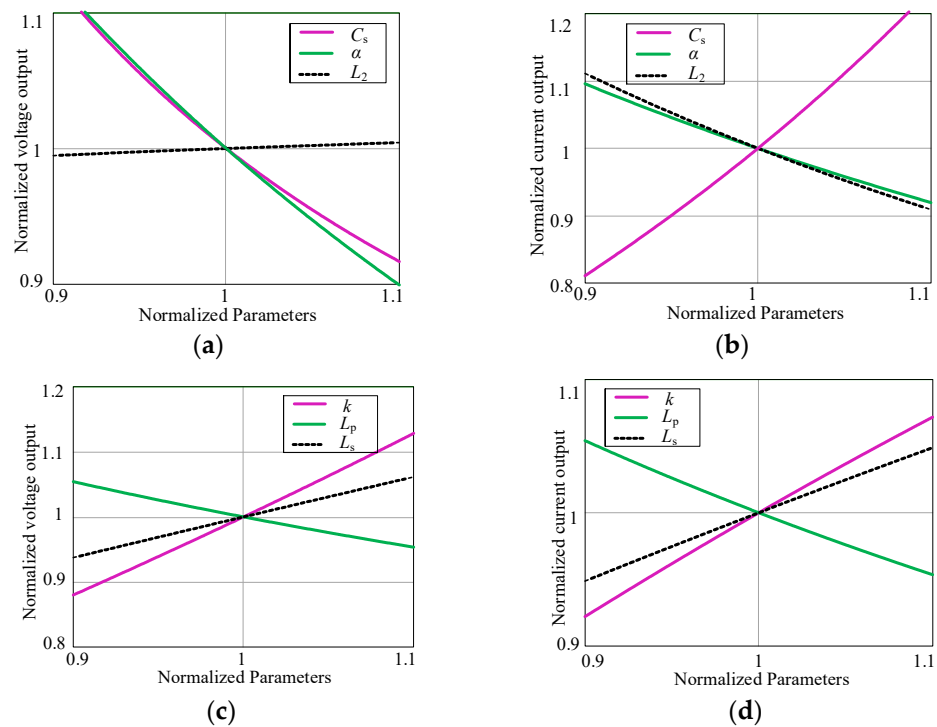


**Figure 8.** The variation of output with  $C_s$ ,  $\alpha$ , and  $L_2$ . (a,c) CV mode; (b,d) CC mode of operation.

#### 4. Experiment Results

To verify the correctness of the above analysis and the feasibility of the proposed topology, a 180 W wireless charging prototype with 60 V/3 A was built using the proposed topology, as shown in Figure 9. The prototype is composed of an inverter unit, a transmitting coil, a receiving coil, and a rectifier marked as 1–4 in turn. Figure 10a,b present the  $u_{ds}$  and  $u_{gs}$  in both CC mode and CV mode.

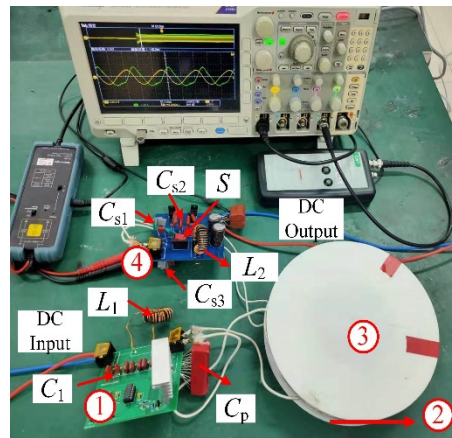


Figure 9. Wireless charging prototype using proposed topology.

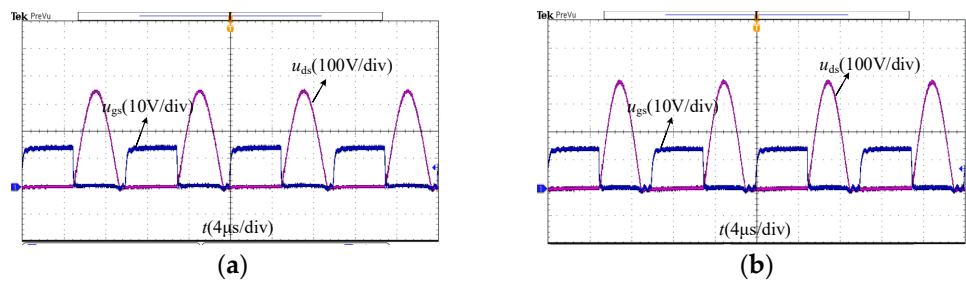


Figure 10. The  $u_{ds}$  and  $u_{gs}$  in CC and CV mode. (a) CC mode; (b) CV mode.

As seen in Figure 10, both modes achieved ZVS, and the blocking voltage of the switch in CC mode is smaller than that of CV mode by 25 V. Figure 11a,b show the waveform of output voltage and current as the power turns from full-power to half-power and then back to full-power in two modes, respectively.

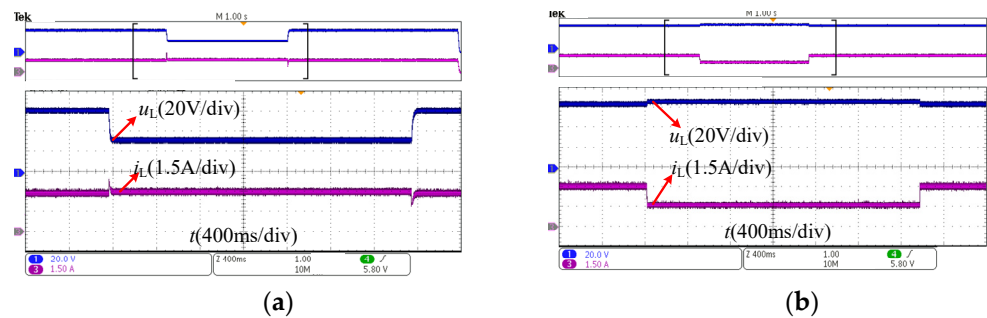


Figure 11. Waveform of output voltage and current. (a) Load  $20\ \Omega$ - $10\ \Omega$ - $20\ \Omega$  changes in CC mode; (b) load  $20\ \Omega$ - $40\ \Omega$ - $20\ \Omega$  changes in CV mode.

As shown in Figure 11, with the change of the load,  $i_L$  in CC mode remains at 3 A, and  $u_L$  in CV mode is kept at 60 V. The CC and CV output characteristic is well achieved.

Figure 12 shows the dynamic performance of the system at the load of  $20\ \Omega$ . The output voltage and current change relatively swiftly when the system switches from CC mode to CV mode, and the dynamic response is fast.

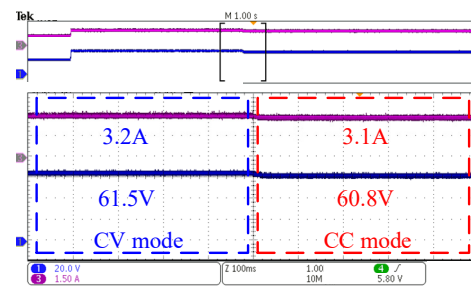


Figure 12. Dynamic performance of the system when the load is 20 Ω.

The measured and theoretical output voltage and current at different loads are shown in Figure 13.

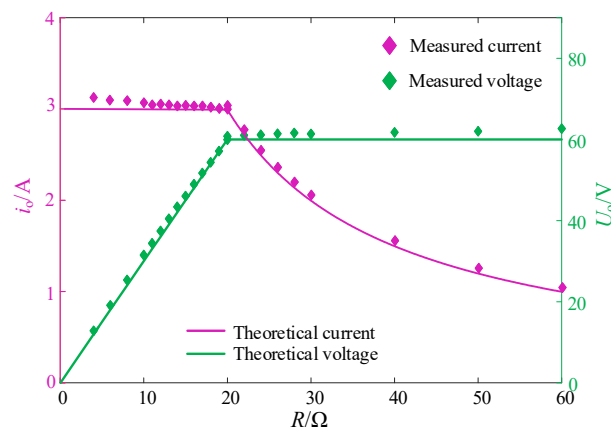


Figure 13. Theoretical and measured values of output voltage and current.

Finally, the curve of efficiency from the DC power source to the resistive load processed can be seen in Figure 14. It can be seen from the results that the max efficiency of CC mode is 89.5% and that of CV mode is 90.3%. Efficiency increases when the mode switches, which is because the output power will increase when it changes from CC mode to CV mode.

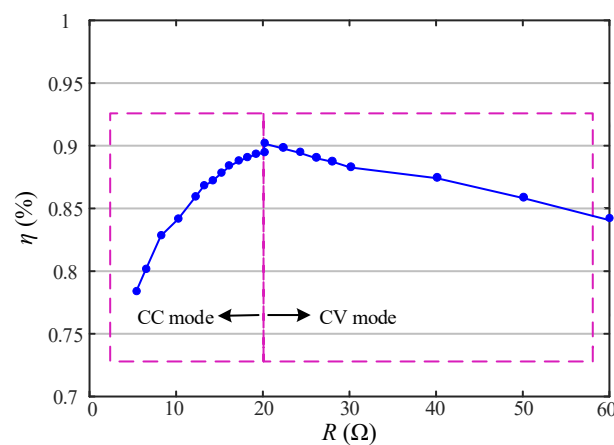


Figure 14. System efficiency graph.

The operating performances of this paper were compared with the WPT system using Class E topology, which is shown in Table 2.

**Table 2.** Comparison of WPT system using Class E topology.

Topology	Frequency	Output Power	Efficiency	CC/CV
Proposed	100 kHz	180 W	90.3%	Yes
[6]	6.78 MHz	30 W	80%	Yes
[9]	6.78 MHz	39.7 W	81.4%	No
[20]	1 MHz	3 W	79.6%	No
[21]	1 MHz	27.8 W	74.7%	No
[22]	13.56 MHz	25.6 W	73.4%	No

It is clear from Table 2 that Class E topology is mainly applied in MHz-frequency and low-power applications of WPT. The work detailed in this paper expands its application range and achieves higher output power and efficiency. In addition, compared with [4], a simpler method is adopted to achieve CC and CV output.

## 5. Conclusions

In this paper, a novel hybrid Class E topology with load-independent output was proposed. Compared to the traditional Class E topology, this hybrid topology presented in this paper can transmit higher power and realize the load-independent output characteristics only by switching the branch once, characterized by the strength of fewer components, simple control, and high reliability. The topology parameters were designed in detail. To improve the design freedom, the compensation method of manually separating the transmitting coils is used, which can also be applied to other WPT systems. Moreover, the relationship between the system parameters and the sensitivity of the topology was analyzed. Finally, a 180 W wireless charging prototype with 60 V/3 A was built using the proposed topology; the experimental results showed perfect agreement with the theoretical analysis and confirmed the feasibility of our novel approach.

**Author Contributions:** B.P.: methodology, software, validation, investigation, resources, writing—original draft preparation. H.L.: conceptualization, formal analysis, data curation, writing—review and editing, visualization, Y.W.: project administration, J.L.: supervision. All authors have read and agreed to the published version of the manuscript.

**Funding:** This research received no external funding.

**Institutional Review Board Statement:** Not applicable.

**Informed Consent Statement:** Not applicable.

**Data Availability Statement:** Not applicable.

**Conflicts of Interest:** The authors declare no conflict of interest.

## References

- Li, H.; Yang, Y.; Chen, J.; Xu, J.; Liu, M.; Wang, Y. A Hybrid Class-E Topology with Constant Current and Constant Voltage Output for Light EVs Wireless Charging Application. *IEEE Trans. Transp. Electr.* **2021**, *7*, 2168–2180. [[CrossRef](#)]
- Kazmierkowski, M.P.; Moradewicz, A.J. Contactless energy transfer (CET) systems—A review. In Proceedings of the 2012 15th International Power Electronics and Motion Control Conference (EPE/PEMC), Novi Sad, Serbia, 4–6 September 2012.
- Wang, Y.; Yao, Y.; Liu, X.; Xu, D.; Cai, L. An LC/S compensation topology and coil design technique for wireless power transfer. *IEEE Trans. Power Electron.* **2018**, *33*, 2007–2025. [[CrossRef](#)]
- Li, H.; Wang, C.; Liu, Y.; Yue, R. Research on single-switch wireless power transfer system based on SiC MOSFET. *IEEE Access* **2019**, *7*, 163796–163805. [[CrossRef](#)]
- Kuperman, A.; Levy, U.; Goren, J.; Zafransky, A.; Savernin, A. Battery charger for electric vehicle traction battery switch station. *IEEE Trans. Ind. Electron.* **2013**, *60*, 5391–5399. [[CrossRef](#)]
- Liu, S.; Liu, M.; Yang, S.; Ma, C.; Zhu, X. A novel design methodology for high-efficiency current-mode and voltage-mode class-e power amplifiers in wireless power transfer systems. *IEEE Trans. Power Electron.* **2017**, *32*, 4514–4523. [[CrossRef](#)]
- Nagashima, T.; Wei, X.; Bou, E.; Alarcón, E.; Kazimierzczuk, M.K.; Sekiya, H. Steady-State analysis of isolated Class-E<sup>2</sup> converter outside nominal operation. *IEEE Trans. Ind. Electron.* **2017**, *64*, 3227–3238. [[CrossRef](#)]
- He, L.; Guo, D. Compound voltage clamped class-e converter with ZVS and flexible power transfer for WPT system. *IEEE Trans. Power Electron.* **2020**, *35*, 7123–7133. [[CrossRef](#)]

9. Oh, H.; Lee, W.; Koo, H.; Bae, J.; Hang, K.C.; Lee, K.; Yang, Y. 6.78 MHz wireless power transmitter based on a reconfigurable Class-E power amplifier for multiple device charging. *IEEE Trans. Power Electron.* **2020**, *35*, 5907–5917. [[CrossRef](#)]
10. Song, K.; Wei, R.; Yang, G.; Zhang, H.; Li, Z.; Huang, X.; Jiang, J.; Zhu, C.; Du, Z. Constant current charging and maximum system efficiency tracking for wireless charging systems employing dual-side control. *IEEE Trans. Ind. Appl.* **2020**, *56*, 622–634. [[CrossRef](#)]
11. Li, S.; Li, W.; Deng, J.; Nguyen, T.D.; Mi, C.C. A double-sided lcc compensation network and its tuning method for wireless power transfer. *IEEE Trans. Veh. Technol.* **2015**, *64*, 2261–2273. [[CrossRef](#)]
12. Zhou, S.; Mi, C.C. Multi-Paralleled LCC reactive power compensation networks and their tuning method for electric vehicle dynamic wireless charging. *IEEE Trans. Ind. Electron.* **2016**, *63*, 6546–6556. [[CrossRef](#)]
13. Tsaramirsis, G.; Papoutsidakis, M.; Derbali, M.; Khan, F.Q.; Michailidis, F. Towards Smart Gaming Olfactory Displays. *Sensors* **2020**, *20*, 1002. [[CrossRef](#)] [[PubMed](#)]
14. Li, Y.; Hu, J.; Lin, T.; Li, X.; Chen, F.; He, Z.; Mai, R. A new coil structure and its optimization design with constant output voltage and constant output current for electric vehicle dynamic wireless charging. *IEEE Trans. Ind. Electron.* **2019**, *15*, 5244–5256. [[CrossRef](#)]
15. Qu, X.; Han, H.; Wong, S.; Tse, C.K.; Chen, W. Hybrid IPT topologies with constant current or constant voltage output for battery charging applications. *IEEE Trans. Power Electron.* **2015**, *30*, 6329–6337. [[CrossRef](#)]
16. Chen, Y.; Li, M.; Yang, B.; Chen, S.; Li, Q.; He, Z.; Mai, R. Variable-Parameter T-Circuit-Based IPT System Charging Battery with Constant Current or Constant Voltage Output. *IEEE Trans. Power Electron.* **2020**, *35*, 1672–1684. [[CrossRef](#)]
17. Chen, Y.; Xiao, W.; Guan, Z.; Zhang, B.; Qiu, D.; Wu, M. Nonlinear modeling and harmonic analysis of magnetic resonant WPT system based on equivalent small parameter method. *IEEE Trans. Ind. Electron.* **2019**, *66*, 6604–6612. [[CrossRef](#)]
18. Aldhaher, S.; Luk, P.C.; Bati, A.; Whidborne, J.F. Wireless power transfer using class e inverter with saturable DC-Feed inductor. *IEEE Trans. Ind. Appl.* **2014**, *50*, 2710–2718. [[CrossRef](#)]
19. Zhang, W.; Mi, C.C. Compensation Topologies of High-Power Wireless Power Transfer Systems. *IEEE Trans. Veh. Technol.* **2016**, *65*, 4768–4778. [[CrossRef](#)]
20. Zhang, X.; Zhang, X.; Yao, Y.; Yang, H.; Wang, Y.; Xu, D. High-efficiency magnetic coupling resonant wireless power transfer system with class-e amplifier and class-e rectifier. In Proceedings of the 2017 IEEE Transportation Electrification Conference and Expo, Asia-Pacific (ITEC Asia-Pacific), Harbin, China, 7–10 August 2017; pp. 1–5.
21. Liu, M.; Fu, M.; Wang, Y.; Ma, C. Battery cell equalization via megahertz multiple-receiver wireless power transfer. *IEEE Trans. Power Electron.* **2018**, *33*, 4135–4144. [[CrossRef](#)]
22. Chen, W.; Chinga, R.A.; Yoshida, S.; Lin, J.; Chen, C.; Lo, W. A 25.6 W 13.56 MHz wireless power transfer system with a 94% efficiency GaN Class-E power amplifier. In Proceedings of the 2012 IEEE/MTT-S International Microwave Symposium Digest, Montreal, QC, Canada, 17–22 June 2012; pp. 1–3.